Bioactive Materials 33 (2024) 242–250

Contents lists available at ScienceDirect

Bioactive Materials

journal homepage: www.keaipublishing.com/en/journals/bioactive-materials

Zn-Fe primary battery-enabled controlled hydrogen release in stomach for improving insulin resistance in obesity-associated type 2 diabetes

Boyan Liu [a,1], Peixun Lv [a,b,1], Xiaoyi Zhang [a], Chao Xia [c], Xinru Liu [a], Jingyu Liu [a], Junli Xue [a], Qianjun He [b,d,*], Shucun Qin [a,**]

[a] Key Laboratory of Major Diseases and Hydrogen Medical Translational Applications in Universities of Shandong Province & Key Laboratory of Hydrogen Biomedical Research of Health Commission of Shandong Province, Taishan Institute for Hydrogen Biomedical Research, The Second Affiliated Hospital of Shandong First Medical University, Tai'an, 271000, China

[b] Shanghai Key Laboratory of Hydrogen Science & Center of Hydrogen Science, School of Materials Science and Engineering, Shanghai Jiao Tong University, Shanghai, 200240, China

[c] School of Biomedical Engineering, Medical School, Shenzhen University, Shenzhen, 518060, China

[d] Shenzhen Research Institute, Shanghai Jiao Tong University, Shenzhen, 518057, China

ARTICLE INFO

Keywords:
Hydrogen therapy
Primary battery
Type 2 diabetes
Insulin resistance
Anti-inflammation

ABSTRACT

Chronic systemic inflammation in obesity-associated type 2 diabetes (T2D) is a key inducing factor of insulin resistance (IR). Hydrogen molecule (H_2) has been proved to be a safe and effective anti-inflammatory agent, but conventional H_2 administration methods cannot provide a high dosage and a long duration of H_2 treatment in IR-related tissues and thus lead to limited therapeutic efficacies. We here propose a new strategy of controlled H_2 release to match the time window of gastric emptying for maximizing the bioavailability and therapeutic outcome of H_2. This work enhances the hydrolysis rate of Zn by constructing a Zn-Fe primary-battery micro-/nano-structure, and the H_2-releasing rate is adjusted by tuning the ratio of Zn to Fe. The Zn-Fe micro-/nano-structure is orally administrated once daily to alleviate obesity-associated T2D in a leptin-deficient (*ob*/*ob*) mouse model. The H_2 generation time of the Zn-Fe primary-battery micro-/nano-structure with the Fe/Zn ratio of 1:100 in gastric acid is about 3 h, just matching with the time window of gastric emptying in mice. *In vivo* monitoring results show that H_2 generated by Zn-Fe micro-/nano-structure in stomach can effectively accumulate in major IR-sited tissues including liver, adipose tissue, and skeletal muscle at a high dose for a relatively long time compared to H_2-rich water drinking. Oral administration of Zn-Fe micro-/nano-structure at 200 mg/kg body weight has realized an efficient IR improvement and remarkably ameliorated systemic inflammation in *ob*/*ob* mice. In addition, a high-dose administration of Zn-Fe shows no visible toxicity in mice. This work provides a new strategy to maximize the outcome of hydrogen therapy.

1. Introduction

Type 2 diabetes (T2D) is a serious health problem globally and it is estimated that 439 million people would catch T2D by 2030 [1]. It is well known that T2D is a chronic metabolic disorder highly interrelated with obesity. In the progression of obesity-associated T2D, insulin resistance (IR) frequently causes target cells fail to normally respond to insulin [2]. Increasing evidences indicate that chronic systemic inflammation is a key factor of inducing IR. Typically, sustaining inflammation in liver, adipose tissue, and skeletal muscle locally causes IR by inhibiting insulin signal transduction [3]. Thus, it is promising to develop broad-spectrum anti-inflammatory agents targeting multiple IR-sited tissues for effective anti-IR.

Generally, lifestyle interventions for weight reduction are adopt to improve IR, but it is difficult for individuals to insist, and therefore pharmacological management is frequently needed. Current

Peer review under responsibility of KeAi Communications Co., Ltd.

* Corresponding author. Shanghai Key Laboratory of Hydrogen Science & Center of Hydrogen Science, School of Materials Science and Engineering, Shanghai Jiao Tong University, Shanghai, 200240, China.

** Corresponding author.

E-mail addresses: nanoflower@126.com (Q. He), scqin@sdfmu.edu.cn (S. Qin).

[1] These authors contributed equally to this work.

https://doi.org/10.1016/j.bioactmat.2023.11.003

Received 1 September 2023; Received in revised form 16 October 2023; Accepted 7 November 2023

pharmacological agents against IR mainly include metformin (Met) and pioglitazone [4]. However, both drugs have certain side effects in the incident of gastrointestinal adverse events and edema [5,6], so that their anti-IR efficacies are hardly sustainable in a long run [4]. Therefore, there is an urgent need to develop safe and effective anti-IR new technologies.

Hydrogen molecule (H_2) has been proved to be a safe, effective and broad-spectrum anti-inflammatory agent which brings benefits for many inflammation-related diseases including metabolic diseases [7,8], cancer [9], and nervous system disorders in clinical researches [10]. Oral administration of H_2-rich water (HRW) is found to be able to improve glucose metabolism in T2D patients and animal models [11–13], but the amount of H_2 delivered by water is rather low because the saturated solubility of H_2 in water is considerably low (0.8 mmol/L at room temperature and normal pressure) and the daily uptake amount of water is limited. The development of solid H_2 donors such as metal hydrides, borides and silicides will favor to enhance the efficiency of H_2 delivery [14–19]. Several oral agents of H_2 donor have been developed to enhance the efficiency of H_2 delivery, but there are still many issues. Oral administration of H_2 producing materials such as magnesium (Mg) microparticles, magnesium hydride (MgH_2) microparticles, calcium hydride (CaH_2) microparticles, iron (Fe) nanoparticles and ammonia borane (AB) encapsulated hollow mesoporous silica nanoparticles (AB@hMSN) is convenient and can support a high H_2-dose [20], but their H_2-releasing rates in gastric acid is either too fast (Mg, MgH_2, CaH_2, and AB@hMSN) or too low (Fe and Zn) compared with the time window of gastric emptying (about 4 h for human [21] and 3 h for mice [22]). Thus, it is a big challenge to control their H_2-releasing rates for matching with the time window of gastric emptying in order to maximize the bioavailability and therapeutic outcome of H_2.

Herein, we proposed a primary-battery strategy to construct a new kind of Zn-Fe micro-/nano-structure, realizing the controlled acid-responsive H_2 release and adjusting the H_2 releasing duration within the time window of gastric metabolism (Scheme 1). *In vivo* monitoring results showed that H_2 generated by Zn-Fe in stomach can effectively accumulate in major IR-sited tissues including liver, adipose tissue, and skeletal muscle at a high dose for a relatively long time. Oral administration of Zn-Fe once daily can ameliorate the obesity-related inflammation, and realize efficient IR improvement in an obese diabetic leptin-deficient (*ob/ob*) mouse model.

2. Material and methods

2.1. Chemicals

Zn powder, ferric chloride ($FeCl_3$) and zinc oxide (ZnO) all were purchased from Sigma-Aldrich. Ethanol was purchased from Energy Chemical.

2.2. Synthesis and characterization of Zn-Fe and ZnO-Fe_2O_3

The synthesis of Zn-Fe primary battery was based on a displacement reaction. By applying the reducibility of Zn, iron ion was reduced to zero-valent Fe on the surface of Zn microparticles. Details were as follows: 162.2 mg of $FeCl_3$ was dissolved into 50 mL deionized water to form 0.02 mol/L $FeCl_3$ solution. According to the different molar ratios of $FeCl_3$:Zn (10:100, 1:100 and 1:300), 65, 650, and 1950 mg of Zn microparticles were dispersed into 5 mL $FeCl_3$ solution under rapid stirring. After reaction for 10 min, the samples were collected by centrifugation, washed with deionized water and ethanol in turn, and then dried under vacuum to obtain Zn-Fe primary-battery nano/microparticles with different Fe/Zn ratios (Fe:Zn = 10:100, 1:100, and 1:300).

ZnO-Fe_2O_3 was synthesized as a negative control of Zn-Fe. Fe_2O_3 was grown on the ZnO surface by hydrothermal synthesis. The details were as follows: 202.75 mg $FeCl_3$ was dissolved in 1 mL deionized water to form 202.75 mg/mL $FeCl_3$ solution, and 5 mg KH_2PO_4 was dissolved in 1 mL deionized water to form 5 mg/mL KH_2PO_4 solution. Then, 1.017 g ZnO was dispersed in 30 mL deionized water, and then 100 μL of $FeCl_3$ solution and 100 μL of KH_2PO_4 solution were added in turn. After ultrasonic dispersion, the above system was transferred to a polytetrafluoroethylene-lining reactor, whose temperature was increased to 150 °C at a heating rate of 3 °C/min and then maintained at 150 °C for 48 h. After cooling, the sample was washed twice with deionized water, collected by centrifugation at 12,000 rpm, and then freeze-dried to obtain ZnO-Fe_2O_3.

The morphology and size of the Zn-Fe primary battery were characterized by scanning electron microscopy (FEI Apero S). The chemical

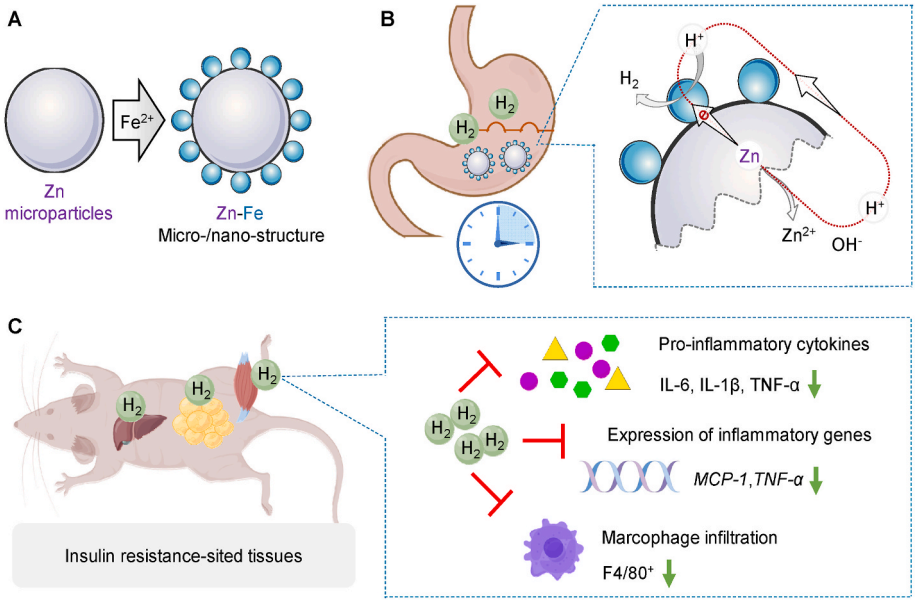

Scheme 1. Schematic illustration for the structure and construction method of the Zn-Fe primary-battery micro-/nano-structure (**A**), the primary-battery principle for accelerated Zn hydrolysis and H_2 generation (**B**), the efficient H_2 accumulation in insulin resistance-sited tissues after oral Zn-Fe administration in support of enhanced anti-inflammation and improved insulin tolerance (**C**).

valence of Zn-Fe primary battery was detected by X-ray photoelectron spectroscopy (XPS). The crystal structure was characterized by X-ray diffraction (PANalytical, Empyrean).

2.3. Measurement of H_2 generation in vitro

Different metal powders (Zn, Fe and Mg) and Zn-Fe nano/microparticles with different Fe/Zn ratios (Fe:Zn = 10:100, 1:100, and 1:300) were added into the phosphate buffer solution (PBS) with a pH value of 1.2 to simulate gastric condition at 37 °C. The release of H_2 was monitored in real time by gas chromatography (Agilent 7890B) [23].

2.4. Pharmacokinetics study

Six to eight-week-old male wild-type (WT) C57BL/6J mice were intragastrically administered with Zn-Fe (20 mg/mL in water) or HRW (0.8 mmol/L H_2 in water) at a dose of 0.1 mL/10 g body weight (BW) (equal to Zn-Fe 200 mg/kg BW). The H_2 concentrations in liver, adipose tissue (epididymal fat pad), and skeletal muscle (gastrocnemius muscle) were monitored in real time by a Clark-type H_2 sensor (Unisense, Aarhus N, Denmark) [24,25]. At the same time, the serum samples were collected at 0, 1, 2, 3, 6, 12, 24, and 48 h ($n = 3$). The quantification of Zn concentration in serum was performed using inductively coupled plasma mass spectrometry (ICP-MS, Agilent 7800, Agilent Technologies, USA).

2.5. Animal experiments

Six to eight-week-old male WT C57BL/6J mice and C57BL/6J-based *ob/ob* mice were purchased from Vital River Laboratory Animal Technology Co., Ltd. (Beijing, China). Mice were housed in a specific pathogen-free facility with a 12/12 h light-dark cycle at 22 °C and given free access to food and water. All animal care and experiments were carried out following protocols approved by the Laboratory Animal Ethics Committee of Shandong First Medical University (No. W202108080304). After 1 week of acclimatization, mice were randomly assigned to six groups (8 mice per group). (I) WT group: WT mice intragastrically administered with water at 0.1 mL/10 g BW once daily; (II) Model group: *ob/ob* mice intragastrically administered with water; (III) ZnO-Fe_2O_3 group: *ob/ob* mice intragastrically administered with aqueous solution of ZnO-Fe_2O_3 at 200 mg/kg BW once daily; (IV) Zn-Fe group: *ob/ob* mice intragastrically administered with aqueous solution of Zn-Fe at 200 mg/kg BW once daily; (V) HRW group: *ob/ob* mice administered with HRW *ad libitum* (about 1.5 mL HRW, 0.6–1.5 μmol/10 g daily H_2 administrated amount) and intragastrically administered with water; (VI) Met group: *ob/ob* mice intragastrically administered with aqueous solution of Met at 200 mg/kg BW once daily. The mice received oral glucose tolerance test (OGTT) and insulin tolerance test (ITT) after 11 weeks and were sacrificed after 12 weeks (Fig. S1).

Blood samples were collected in EDTA-coated tubes, centrifuged at 3000 rpm for 15 min at 4 °C, and the plasma was stored at −80 °C. A portion of liver, gastrocnemius muscle, inguinal white adipose tissue, and pancreas were rapidly excised, dipped in liquid nitrogen, and stored at −80 °C for further analysis or fixed in 4% paraformaldehyde for 24 h for histological studies.

2.6. HRW drinking

Mice in HRW group were provided with HRW *ad libitum*. HRW was prepared in an HRW-producing apparatus (ZQLH-F-150G, Zhongqinglianhe Tech Co., Ltd, Liaocheng, China), and stored in a drinking bottle with stainless steel balls in the outlet. The concentration of H_2 in HRW was monitored using a Clark-type H_2 microsensor (Unisense, Aarhus N, Denmark). HRW was replaced with freshly prepared one every 8 h to ensure that the concentration of H_2 was above 600 μmol/L [26].

2.7. Toxicity assessment

Six to eight-week-old male C57BL/6J mice were randomly divided into four groups (12 mice per group) and intragastrically administered with water (vehicle) or Zn-Fe at 200, 400, and 800 mg/kg BW every day. Six mice in each group were sampled after 1 or 2 weeks. Blood samples were collected for biochemical tests. Major organs including stomach, small intestine, liver, kidney, spleen, and heart were dissected, fixed in 4% paraformaldehyde, and embedded into paraffin for further hematoxylin & eosin (H&E) staining.

2.8. Biochemical analysis

Total cholesterol (TC) and triglyceride (TG) in plasma and liver were measured with commercial kits (Nanjing Jiancheng Bioengineering Institute, Nanjing, Jiangsu, China). Plasma levels of insulin, tumor necrosis factor (TNF)-α, interleukin (IL)-6, IL-1β, and c-reactive protein (CRP) were measured using corresponding ELISA kits (Mlbio, Shanghai, China). A bicinchoninic acid protein assay kit (Solarbio Science & Technology Co., Ltd., Beijing, China) was used to determine the protein content in various tissues.

2.9. Oral glucose tolerance test and insulin tolerance test

The OGTT was performed by detecting the blood glucose levels at 0, 15, 30, 60, and 120 min after oral gavage of 2 g/kg glucose to the 12 h fasted mice. The ITT was performed by detecting the blood glucose levels at 0, 15, 30, 60, and 120 min after intraperitoneal injection of 0.75 U/kg insulin to the 4 h fasted mice. The glucose levels were determined in blood drops obtained by clipping the tail of the mice using OneTouch Ultra Mini glucometer (LifeScan; Milpitas, CA, USA).

2.10. Immunohistochemistry and immunofluorescence

Adipose tissue and liver samples embedded in paraffin were stained for expression of F4/80 with an anti-F4/80 monoclonal antibody (ab111101, Abcam, Cambridge, MA, USA, 1:100) according to the standard histological procedure ($n = 6$ in each group). The immunoreactive cells were counted in five visual field under a 400 × light microscope. Immunofluorescence was performed with primary antibodies, including insulin (gb13121, Servicebio, 1:300) and glucagon (gb11097, Servicebio, 1:200). The percentage of β-cell area in the pancreas was calculated by dividing the area of all insulin-positive cells by the whole area of this section ($n = 4$ in each group).

2.11. Quantitative real-time PCR

Adipose tissue, skeletal muscle, liver, and pancreas samples were homogenized and total RNA was extracted with TRIzol. The cDNA was produced in an ABI Veriti 96 Well Thermal Cycler (Waltham, MA, USA) using HiFiScript cDNA Synthesis kit from CWBIO (Beijing, China). Quantitative real-time PCR was performed in an ABI QuantStudio3 PCR System (Waltham, MA, USA) using SYBR Green qPCR Master Mix and gene-specific primers. The $2^{-\Delta\Delta CT}$ method was used to normalize mRNA expression level to that of the endogenous housekeeping gene peptidylprolyl isomerase A (*PPIA*). This experiment was repeated four times independently. The primer sequences were as follows: *TNF-α*, 5′-GAACTGGCAGAAGAGGCACT-3’ (forward) and 5′-GGTCTGGGCCATAGAACTGA-3’ (reverse); *IL-6*, 5′-CCGGAGAGGAGACTTCACAG-3’ (forward) and 5′-TTCTGCAAGTGCATCATCGT-3’ (reverse); monocyte chemoattractant protein-1 (*MCP-1*), 5′-CCCAATGAGTAGGCTGGAGA-3’ (forward) and 5′-TCTGGACCCATTCCTTCTTG-3’ (reverse); *PPIA*, 5′-GACCAAACACAAACGGTTCC-3’ (forward) and 5′-CATGCCTTCTTTCACCTTCC-3’ (reverse); insulin receptor substrate 2 (*Irs2*), 5′-ACAACAACCACAGCGTGCGC-3’ (forward) and 5′-GTAGAGGGCGATCAGGTACTTG-3’ (reverse); insulin receptor (*Insr*), 5′-

AGGCTCCCGTCTCTTCTTCAA-3' (forward) and 5′-GACATCCCCA-CATTCCTCGTT-3' (reverse); pancreatic and duodenal homeobox 1 (*Pdx1*), 5′-TTCCCGAATGGAACCGAGC-3' (forward) and 5′-GTAGG-CAGTACGGGTCCTCT-3' (reverse); and insulin like growth factor 1 receptor (*Igf1r*), 5′-TCCCTCAGGCTTCATCCGCAA-3' (forward) and 5′-CTTCAGCTTTGCAGGTGCACG-3' (reverse).

2.12. Transcriptomic analysis

Total RNA was extracted from stomach and small intestine using a Trizol reagent according to the manufacturer's instructions. RNA samples were detected based on the A260/A280 absorbance ratio with a Nanodrop ND-2000 system (Thermo Scientific, USA), and the RNA integrity number was determined by an Agilent Bioanalyzer 4150 system (Agilent Technologies, CA, USA). Paired-end libraries were prepared using a ABclonal mRNA-seq Lib Prep Kit (ABclonal, China) following the manufacturer's instructions. The mRNA was purified from 1 μg total RNA using oligo (dT) magnetic beads followed by fragmentation carried out using divalent cations at elevated temperatures in ABclonal First Strand Synthesis Reaction Buffer. Adaptor-ligated cDNA was used for PCR amplification. PCR products were purified (AMPure XP system) and library quality was assessed on an Agilent Bioanalyzer 4150 system. Finally, the qualified library was sequenced using an Illumina Novaseq 6000 to obtain raw data. Then clean reads were separately aligned to the mouse reference using HISAT2 software (http://daehwankimlab.github.io/hisat2/) to obtain mapped reads. Differential expression analysis was performed using the DESeq2 (http://bioconductor.org/packages/release/bioc/html/DESeq2.html), and differentially expressed genes (DEGs) were identified as $|\log2(\text{fold change})| > 1$ and *P*-adj <0.05. Gene Ontology (GO) functional classifications and Kyoto Encyclopedia of Genes and Genomes (KEGG) analysis were performed using DAVID (http://david.abcc.ncifcrf.gov/home.jsp).

2.13. Statistical analyses

Data were expressed as mean ± SEM unless otherwise indicated. Student's *t*-test was used to compare the difference between two groups, and one-way ANOVA with Bonferroni's post hoc analysis was used for comparison of more than two groups. $^{*}P < 0.05$; $^{**}P < 0.01$; $^{***}P < 0.001$; ns, no significant difference.

3. Results and discussion

3.1. Synthesis and characterization of Zn-Fe micro/nanoparticles

The traditional H_2-administration routes of H_2-rich water drinking and H_2-rich saline injection can only support a relatively low dose of H_2, and H_2-gas inhalation leads to both a low efficiency of H_2 utilization and a high inconveniency for use [26,27]. In recent years, local generation of H_2 based on nanomedicines is on the rise [16,28,29]. However, for the disease of multi-organ targets such as IR, there are currently no nanomedicine strategy for sufficient and sustained H_2 release in multiple target tissues. Meanwhile, acid-responsive H_2 donors such as Mg, MgH_2, CaH_2, Fe, and Al have been developed, but there are still various deficiencies. In the gastric acid environment, the acid hydrolysis of Mg, MgH_2 and CaH_2 is too rapid to ensure the in-time and full gastric absorption of generated hydrogen gas; both Zn and Fe are too inactive to ensure their efficient utilization for hydrogen generation in stomach; and a high concentration of Al has latent toxic effects on the human body. Therefore, this work proposed to enhance the acid-hydrolysis rate of Zn by constructing a Zn-Fe primary-battery structure, and to adjust the acid-hydrolysis rate of the Zn-Fe primary-battery by tuning the ratio of Zn to Fe for matching with the time window of gastric metabolism.

The Zn-Fe primary battery was prepared using Zn microparticles and $FeCl_3$ as reactants by a displacement reaction. SEM and corresponding element mapping images (Fig. 1A and B) showed that iron nanoparticles were uniformly coated on the surface of zinc particles. Owing to local displacement/deposition, the Fe coating was so stable that it cannot be removed by washing, which is beneficial to form a steady primary-battery structure. Furthermore, XPS patterns of Zn-Fe primary battery suggested that iron was reduced to a zero-valence state on the surface of Zn, confirming the primary battery structure definitely (Fig. 1C and D). By the same displacement method, three samples with different ratios of Fe to Zn were prepared to investigate the effect of Fe/Zn ratio on the rate of H_2 generation. From Fig. 1E, the primary-battery structure can indeed accelerate the hydrolysis of Zn for H_2 generation in a simulated gastric acid solution, and the higher ratio of Fe to Zn caused faster H_2 generation because more primary-battery microstructures were formed between more anodes (Fe nanoparticles) and a cathode (Zn microparticle) (Scheme 1B). From SEM images in Fig. S2, high amounts of Fe/Zn displacement led to the surface corrosion of Zn microparticles to form a porous structure, which might favor the acid hydrolysis of Zn-Fe primary-battery micro/nanoparticles.

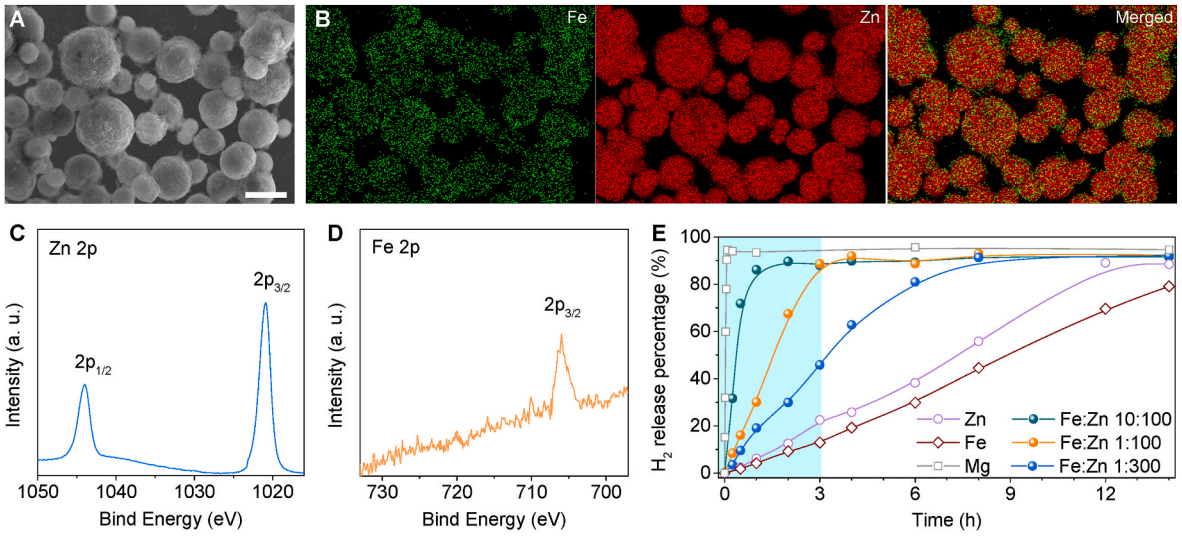

Fig. 1. The representative SEM image (**A**) and corresponding EDS element mapping (**B**) of Zn-Fe micro/nanoparticles, XPS spectra of Zn-Fe micro/nanoparticles (**C**, **D**), and acid-responsive H_2 generation profile of Mg, Fe, Zn, and Zn-Fe micro/nanoparticles with different Fe/Zn ratios in the simulated gastric acid solution (**E**). The scale bar in figure A corresponds to 5 μm.

By comparison, Mg microparticles almost completely decomposed within 5 min in the simulated gastric acid solution (Fig. 1E). Release time duration was so short that the generated H_2 gas can be quickly eructated instead of fully absorbed by stomach. On the other hand, the H_2 generation of both Zn and Fe microparticles was too slow (Fig. 1E). Only when the ratio of Fe to Zn in the Zn-Fe primary battery was 1:100, the time of H_2 generation in the simulated gastric acid solution was just 3 h (Fig. 1E), which can match with the average time period of gastric emptying. Therefore, the Zn-Fe primary battery with this Fe/Zn ratio was used for following therapeutic experiments. Even though there is a different in the time window of gastric metabolism between mice and human being, we can still ensure the match of the acid-hydrolysis rate of the Zn-Fe primary-battery micro-/nano-structure with the time window of gastric metabolism in human being by tuning the ratio of Fe to Zn. Theoretically, the H_2-producing rate of the Zn-Fe primary battery can achieve 30.8 mg/g (375 mL/g) after complete acidolysis, which is far higher than the H_2-loading capacity of saturated HRW (1.6 μg/g). As a control without H_2 generation, the mixture of ZnO and Fe_2O_3 with the same Fe/Zn ratio (1:100) was prepared by a co-precipitation method. The compositions of Zn-Fe and ZnO-Fe_2O_3 were further confirmed by XRD characterization (Fig. S3 and Fig. S4). Additionally, we detected the Zn level in the blood of mice after intragastric administration of Zn-Fe micro/nanoparticles with the Fe/Zn ratio of 1:100 (200 mg/kg) to clarify the *in vivo* metabolic profile. As shown in Fig. S5, the level of Zn in the blood rapidly increased within the first 3 h, and then decreased rapidly to the normal level after 6 h, which was in good accordance with the Zn-Fe hydrolysis progress in stomach and also implied quick metabolism of decomposition products in the body.

3.2. H_2 concentration monitoring in vivo

As a gas molecule with low solubility in water, H_2 gas is characterized with relatively slow dissolution (about 30 min) and exsolution (several hours) rates. Therefore, the sustained H_2 release behavior of the developed Zn-Fe primary-battery micro/nanoparticles were expected in favor of achieving a high bioavailability of H_2 in the stomach. The *in vivo* dynamic curves for H_2 concentrations in the stomach wall and three IR-related tissues of interest (liver, adipose tissue, and skeletal muscle) were locally detected in real time by a hydrogen microelectrode after intragastric administration of Zn-Fe micro/nanoparticles with the optimal Fe/Zn ratio of 1:100 (200 mg/kg). Meanwhile, oral administration of freshly-prepared saturated HRW (0.8 mM, 10 mL/kg BW) was used as a control to check the advantages of the Zn-Fe primary-battery micro/nanoparticles.

H_2 concentration in the stomach wall quickly exceeded 200 μmol/L in 10 min (Fig. S6), possibly because H_2 generation from the acid hydrolysis of Zn-Fe occurred in the stomach. In general, H_2 concentrations rose rapidly, reached the highest values of 95.8, 102.0, and 1.7 μmol/L in liver (Fig. 2A), adipose tissue (epididymal fat pad) (Fig. 2B), and skeletal muscle (gastrocnemius muscle) (Fig. 2C) in 20.0, 15.0, and 7.5 min after Zn-Fe administration, respectively. Then H_2 concentrations decreased gradually, and still retained over 13.8%, 15.1% and 6.1% of the highest value after 6 h. Such high H_2 concentration and retention duration in investigated tissues, especially liver and adipose tissue, should be attributed to a high H_2-generating capability of Zn-Fe and a higher solubility of H_2 in fat than in water (high lipophilicity). Inhalation of H_2 gas has been widely investigated in basic and clinical studies, but it is not convenient for practical use and H_2 concentration in the liver quickly decreased by 90% in 5 min after H_2 gas inhalation was suspended [24,25]. In comparison, oral administration of Zn-Fe seems more convenient and effective.

Compared with Zn-Fe micro/nanoparticles, intragastric administration of HRW supplied a remarkably lower H_2 concentration and a shorter duration of H_2 in various tissues. In the liver (Fig. 2D), adipose tissue (epididymal fat pad) (Fig. 2E), and skeletal muscle (gastrocnemius muscle) (Fig. 2F), the highest H_2 concentrations were only 3.0, 4.3, and 0.45 μmol/L in 6.3, 4.5, and 4.5 min after HRW administration, and H_2 concentrations decreased by about 95% in 1 h in these three tissues. The speed to achieve the peak value of H_2 concentration in tissues was faster compared with Zn-Fe administration, possibly because HRW saved the dissolution time of H_2 gas. But the peak value of H_2 concentration in tissues was much lower and the half-life time of H_2 in tissues was also remarkably shorter compared with Zn-Fe administration, possibly owing to the lower H_2 dose supplied by HRW. Taking together, the above results indicated that oral administration of the developed Zn-Fe primary-battery micro/nanoparticles can ensure a high H_2 concentration and a long retention duration in major IR-sited tissues and therefore might be especially suitable to anti-IR in obesity-associated T2D.

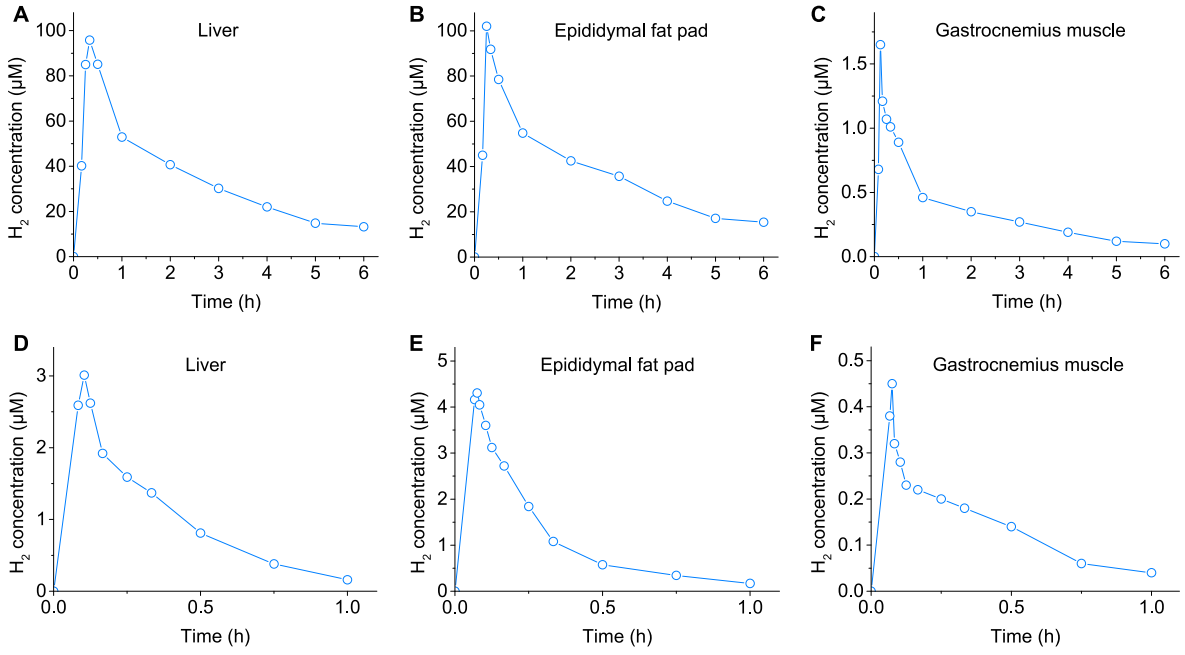

Fig. 2. *In vivo* monitoring of H_2 concentration in liver (**A**, **D**), epididymal fat pad (**B**, **E**), and gastrocnemius muscle (**C**, **F**) after intragastric administration with Zn-Fe micro/nanoparticles with the Fe/Zn ratio of 1:100 (200 mg/kg) (**A**–**C**) or HRW (800 μM, 10 mL/kg) (**D**–**F**).

3.3. Sustained H_2 supply ameliorates obesity and hyperlipidemia in ob/ob mice

To examine the therapeutic potential of Zn-Fe primary-battery micro/nanoparticles in obesity-associated T2D, we used leptin-deficient *ob/ob* mice as a model to mimic the conditions of obesity and T2D development [30], while wild-type C57 mice (WT) without development of obesity and T2D were used as a normal control. As demonstrated in Fig. S1, oral administration of Zn-Fe (200 mg/kg), ZnO-Fe_2O_3 (200 mg/kg), HRW (0.8 mM, 10 mL/kg), and Met (200 mg/kg) once daily were set as therapeutic group, non-hydrogen control group, HRW control group, and Met control group, respectively, to compare the therapeutic outcome of Zn-Fe with traditional therapies. The body weight of mice was monitored every week, and several key parameters including total cholesterol (TC) and triglyceride (TG) levels in plasma and liver, the dimension of adipose cells and the liver/body weight ratio were measured at the end of treatment (12 weeks) to evaluate therapeutic outcomes.

From Fig. 3A, it can be found that the mice body weight of model group increased much faster than that of WT group, reflecting the successful model establishment. At the end of treatment, compared with the model group, Zn-Fe and Met treatments reduced body weight by 6.9% and 4.1%, respectively, whereas HRW treatment had no significant effect on body weight (Fig. 3A). Meanwhile, there was no significant difference in the food uptake amount of *ob/ob* mice between treatment groups and the control group (Fig. S7). Both Zn-Fe and HRW treatments significantly decreased plasma TC levels (Fig. 3B), but only Zn-Fe treatment significantly decreased plasma TG (Fig. 3C). Compared with model group, there was a significant reduction of adipocyte size in inguinal white adipose tissue in Zn-Fe, HRW and Met groups, which was quantitatively reflected as the dimension of adipose cells per field (Fig. 3D and E). Both Zn-Fe and HRW effectively reduced the liver/body weight ratio of mice (Fig. 3F and G). In addition, both the number of round fat vacuoles and the swelling of hepatocytes in the liver tissue of mice were clearly reduced by Zn-Fe treatment (Fig. 3H). Supporting this, the hepatic TC (Fig. S8) and TG (Fig. S9) values were also lowered by both Zn-Fe and HRW treatments. ZnO-Fe_2O_3, which cannot generate H_2 and served as a negative control, showed no functional effect. Metformin (Met), which was used as positive control, resulted in a similar therapeutic effect with Zn-Fe treatment. But Zn-Fe can bring more benefit for body weight reduction than Met. By comparison with HRW, Zn-Fe can more significantly reduce both the dimension of adipose cells and the body weight of *ob/ob* mice. Taken together, these results indicated that Zn-Fe can effectively ameliorate obesity, reduce plasma/hepatic lipid levels, and decrease lipid accumulation in both adipose tissue and liver, possibly owing to sustained H_2 release, high-concentration H_2 accumulation and long-term H_2 retention in these target tissues.

3.4. H_2 improves glucose tolerance in ob/ob mice

The *ob/ob* mice will develop severe insulin resistance (IR) with hyperglycemia and hyperinsulinemia, and therefore the therapeutic efficacy of Zn-Fe on glucose homeostasis was evaluated in the present study. For the fasting blood glucose level, Zn-Fe treatment performed best and

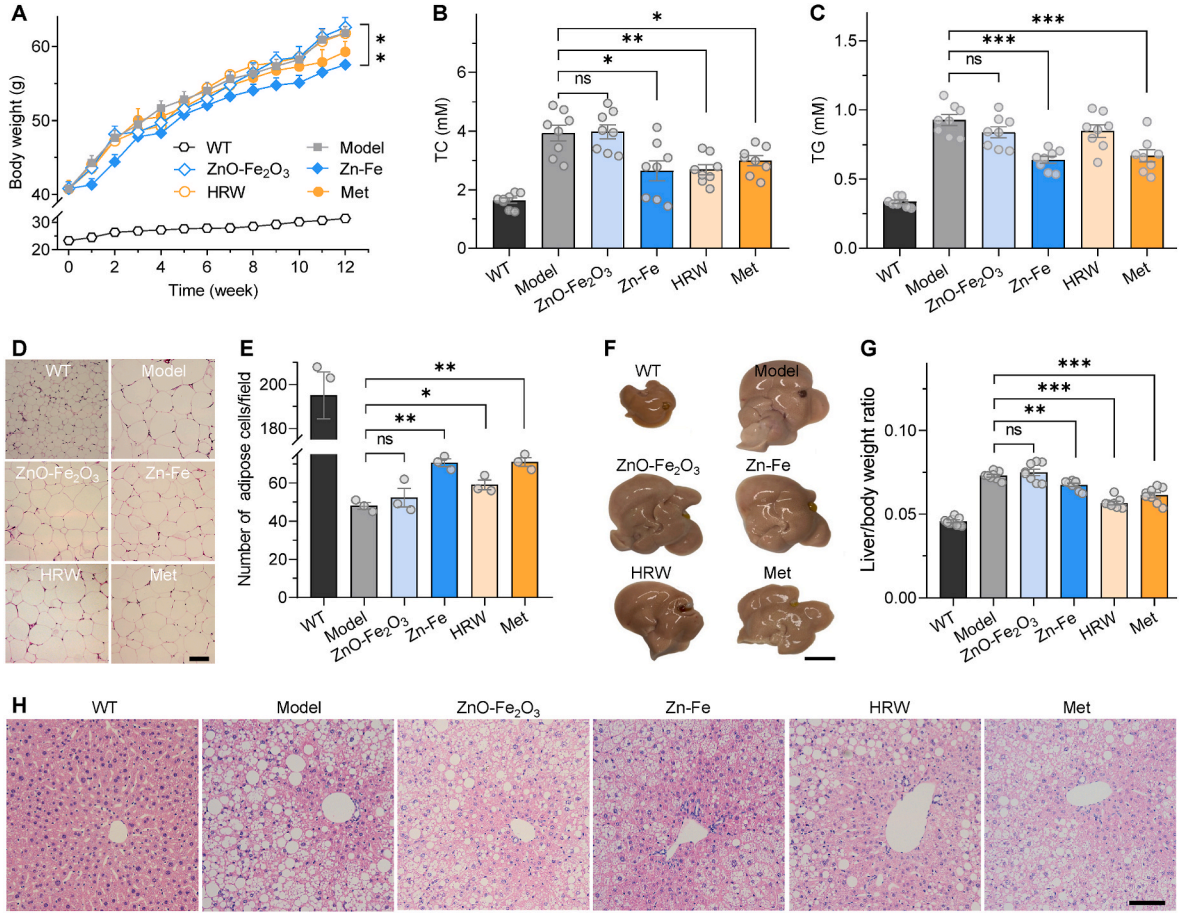

Fig. 3. Sustained H_2 supply ameliorates obesity and hyperlipidemia in *ob/ob* mice. Body weight change during treatment (**A**), plasma TC (**B**, $n = 8$) and TG (**C**, $n = 8$) levels, representative photographs of HE-stained epididymal fat tissue (**D**), the average number of adipocytes (**E**, $n = 3$), representative photographs of liver (**F**), and corresponding liver/body weight ratio (**G**, $n = 8$). The scale bars in figure D, F and H correspond to 100 μm, 1 cm and 100 μm, respectively. Data are shown as mean ± SEM. $^*P < 0.05$, $^{**}P < 0.01$, and $^{***}P < 0.001$.

decreased it by 25.8% compared with the model group (Fig. 4A). Meanwhile, both Zn-Fe and HRW led to a marked improvement in glucose tolerance (Fig. 4A–C). IR is a situation in which insulin sensitivity is reduced. Although neither Zn-Fe nor HRW revealed a significant effect on insulin tolerance (Fig. 4E and F), both of them significantly decreased the plasma insulin level of *ob/ob* mice compared with the model group (Fig. 4D). Especially, the insulin-inhibiting effect of Zn-Fe was remarkably bigger than HRW, resulting in a 42.7% reduction in insulin level (Fig. 4D). Compared with WT, the *ob/ob* mice in the model group had large pancreatic islets and the population of insulin producing β-cells (red fluorescence) distinctly increased (Fig. 4G, Fig. S10). After treatment with Zn-Fe or HRW, islet dimension obviously became smaller and the population of β-cells also clearly decreased (Fig. 4G, Fig. S10). Consistently, Zn-Fe treatment remarkably decreased the mRNA levels of β-cell hyperplasia activators including *Irs2*, *Insr*, *Pdx1*, and *Igf1r* (Fig. S11). This indicated that H_2 can play a compensatory function of insulin islet cells when their function gradually lost in diabetes. Collectively, these data suggested that Zn-Fe treatment could improve glucose tolerance in *ob/ob* mice.

3.5. H_2 ameliorates systemic and tissue proinflammatory responses

Growing evidences have revealed that low-grade systemic inflammation is one of the early and main pathological events that lead to the evolution of IR. H_2 has been proven to exert anti-inflammatory effects in multiple basic and clinical studies. In this study, we explored the effect of Zn-Fe treatment on systemic inflammation in *ob/ob* mice. As expected, the plasma levels of key inflammatory cytokines, IL-6 (Fig. 5A), IL-1β (Fig. 5B), TNF-α (Fig. 5C), and CRP (Fig. S12), were markedly lower in the Zn-Fe group than that in the model group, indicating that systemic inflammation was attenuated by Zn-Fe. Notably, Zn-Fe appeared to work better than HRW. IR and obesity are related to chronic inflammation in metabolic tissues. In this research, Zn-Fe significantly decreased the mRNA expressions of *MCP-1* and *TNF-α* in liver (Fig. 5D), adipose tissue (Fig. 5E), and skeletal muscle (Fig. 5F). Considering the critical role of the activated tissue resident macrophages as a source of cytokines in IR, we next performed immunohistochemical analysis with antibody against F4/80, a macrophage marker. Results showed that macrophage infiltration in liver (Fig. 5G) and adipose tissue (Fig. 5H) was significantly reduced by Zn-Fe treatment compared to the model group. Taken together, these results confirmed that H_2 generated by Zn-Fe in stomach suppressed systemic and tissue inflammation in *ob/ob* mice.

3.6. Transcriptomic analysis of stomach and small intestine

As Zn-Fe reacted with gastric acid in the stomach and then generated H_2 will be absorbed by gastrointestinal tract, we performed transcriptomic analysis of stomach and small intestine to reveal the potential impact of oral Zn-Fe administration. For the stomach, a total of 1065 genes were significantly upregulated and 837 genes were significantly downregulated in the Zn-Fe group compared to the model group (Fig. S13). Gene Ontology (GO) analysis indicated that differentially expressed genes (DEGs) were mainly associated with keratinization, ion transport, fatty acid transport, and lipid metabolic process, *etc.* (Fig. S14). Kyoto Encyclopedia of Genes and Genomes (KEGG) pathway

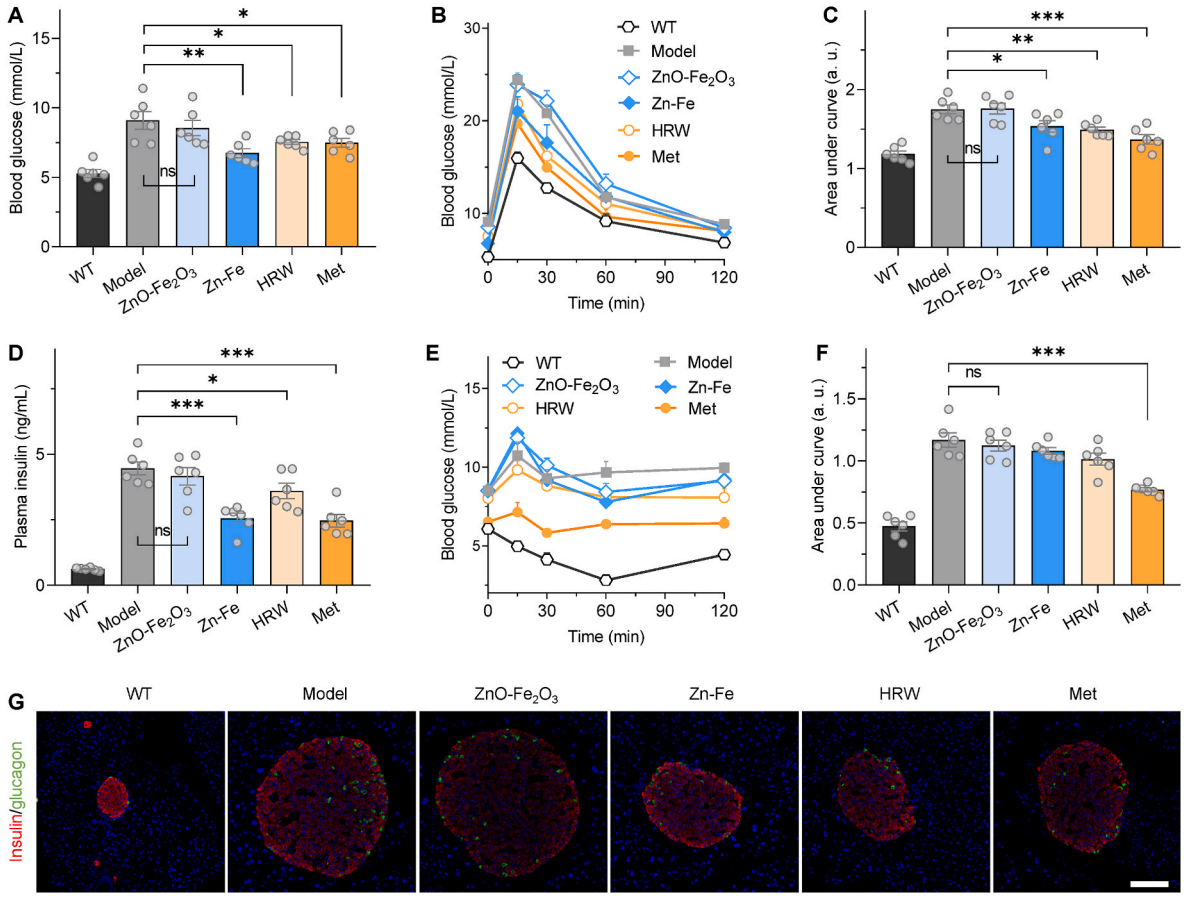

Fig. 4. Sustained H_2 supply improves blood glucose homeostasis. Blood fasting glucose levels (**A**, $n = 6$), oral glucose tolerance test (OGTT) results (**B**), area under curve in OGTT (**C**, $n = 6$), plasma insulin levels (**D**, $n = 6$), insulin tolerance test (ITT) results (**E**), area under curve in ITT (**F**, $n = 6$), immunohistochemical staining of pancreatic sections to detect the expressions of insulin (red) and glucagon (green) (**G**). The scale bar in figure G corresponds to 100 μm. Data are shown as mean ± SEM, $n = 6$ per group. $^*P < 0.05$, $^{**}P < 0.01$, and $^{***}P < 0.001$.

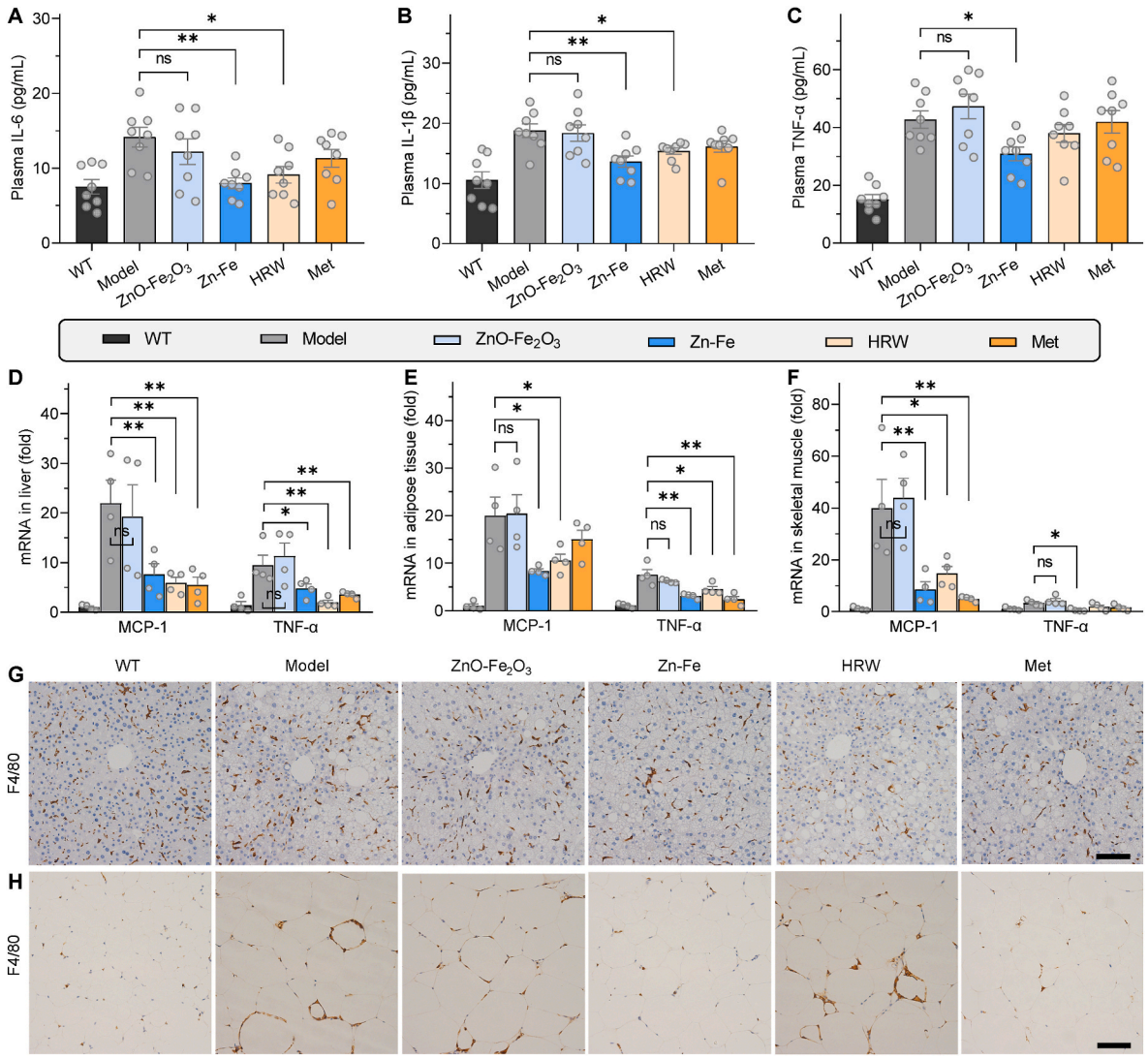

Fig. 5. Sustained H_2 supply alleviates systemic and local inflammatory response. Plasma levels of IL-6 (**A**, $n = 8$), IL-1β (**B**, $n = 8$), and TNF-α (**C**, $n = 8$) after various treatments, relative mRNA expressions of MCP-1 and TNF-α in liver (**D**, $n = 4$), adipose tissue (**E**, $n = 4$), and skeletal muscle (**F**, $n = 4$), immunohistochemical analysis of F4/80 in liver (**G**) and adipose tissue (**H**). The scale bars in figure G and H correspond to 100 μm. Data are shown as mean ± SEM. $^{*}P < 0.05$, $^{**}P < 0.01$, and $^{***}P < 0.001$.

enrichment analysis revealed that the enriched pathways of DEGs in the stomach were mainly related to gastric acid secretion, fat digestion and absorption, cAMP signaling pathway, and vascular smooth muscle contraction, metabolic pathways, insulin secretion, *etc*. (Fig. S15). Meanwhile, Zn-Fe did not show an obvious metabolism-related effect on the small intestine compared to the model group (Fig. S16–S18), possibly because H_2 production by the acid-hydrolysis of Zn-Fe occurred in the stomach rather than in the small intestine. Taking together, these results suggested that besides a high dose of H_2 towards IR-sited tissues for inflammation scavenging and anti-IR, oral administration of Zn-Fe can also directly affect the lipid metabolic function of stomach in *ob/ob* mice.

3.7. *In vivo safety evaluation*

As a new oral formula, the biosafety of Zn-Fe micro/nanoparticles deserves attention. To evaluate the safety of Zn-Fe micro/nanoparticles, C57BL/6J mice were intragastrically administered with blank water or different doses of Zn-Fe micro/nanoparticles with the Fe/Zn ratio of 1:100 (200, 400, and 800 mg/kg) every day. First, there were no significant changes in body weight (Fig. S19) and food-intaking amount (Fig. S20) of the mice treated with various doses of Zn-Fe for 1 or 2 weeks compared with the blank control. Moreover, key plasma indicators for liver (ALT, AST, and ALP) (Fig. S21) and kidney (Cr and BUN) (Fig. S22) functions were examined 1 and 2 weeks after oral Zn-Fe administration. All these biochemical assay data were normal at all investigated dosages of Zn-Fe. In addition, there were no histopathological abnormalities in the stomach, small intestine, liver, kidney, spleen and heart of Zn-Fe treated mice (Fig. S23 and Fig. S24). Noticeably, Fe and Zn are two essential trace element and play a key role for some important biological processes. Considering that a high dose administration of Zn-Fe showed no visible toxicity, it is possible for oral Zn-Fe administration to become an efficient and convenient strategy in clinical use.

4. Conclusions

In summary, we developed a kind of Zn-Fe primary battery micro/nanoparticles with an accelerated acid-responsive H_2 release behavior in the stomach by the primary-battery reaction. By adjusting the proportion of Zn and Fe, we controlled the H_2 release rate and realized the sustained H_2-release within the time window of gastric metabolism. Oral

administration of Zn-Fe micro/nanoparticles caused a relatively high H_2 concentration and a long retention of H_2 in several IR-related tissues including liver, skeletal muscles and white adipose tissues. We found that the inflammation of these insulin sensitive tissues was suppressed, and IR was improved in the obesity-associated type 2 diabetic *ob/ob* mice. Meanwhile, oral administration of Zn-Fe micro/nanoparticles showed a high safety profile. These advantages make Zn-Fe micro/nanoparticles hold a high potential clinical translation.

Data availability

Data will be made available on request.

CRediT authorship contribution statement

Boyan Liu: Investigation, Methodology, Writing – original draft. **Peixun Lv:** Investigation, Methodology, Writing – original draft. **Xiaoyi Zhang:** Investigation. **Chao Xia:** Investigation, Methodology. **Xinru Liu:** Investigation. **Jingyu Liu:** Investigation. **Junli Xue:** Investigation. **Qianjun He:** Conceptualization, Funding acquisition, Project administration, Supervision, Writing – review & editing. **Shucun Qin:** Conceptualization, Funding acquisition, Project administration, Supervision, Writing – review & editing.

Declaration of competing interest

The authors declare no conflicts of interest regarding the publication of this paper.

Acknowledgements

This work was supported by the National Natural Science Foundation of China [82172078, 81770855, 82200508]; Academic Promotion Programme of Shandong First Medical University [2019QL010]; National Key Research and Development Program of China [2022YFB3804500]; Shenzhen Science and Technology Program [RCJC20210706092010008]. We thank Figdraw (www.figdraw.com) for providing scientific drawing materials.

Appendix A. Supplementary data

Supplementary data to this article can be found online at https://doi.org/10.1016/j.bioactmat.2023.11.003.

References

[1] L. Chen, D.J. Magliano, P.Z. Zimmet, The worldwide epidemiology of type 2 diabetes mellitus—present and future perspectives, Nat. Rev. Endocrinol. 8 (2012) 228–236.
[2] B. Mlinar, J. Marc, A. Janez, M. Pfeifer, Molecular mechanisms of insulin resistance and associated diseases, Clin. Chim. Acta 375 (1–2) (2007) 20–35.
[3] C. De Luca, J.M. Olefsky, Inflammation and insulin resistance, FEBS Lett. 582 (1) (2008) 97–105.
[4] A.A. Tahrani, Novel therapies in type 2 diabetes: insulin resistance, Pract, Diabetes 34 (5) (2017) 161–166.
[5] G. Belcher, C. Lambert, G. Edwards, R. Urquhart, D.R. Matthews, Safety and tolerability of pioglitazone, metformin, and gliclazide in the treatment of type 2 diabetes, Diabetes Res. Clin. Pract. 70 (1) (2005) 53–62.
[6] A.A. Tahrani, C.J. Bailey, S. Del Prato, A.H. Barnett, Management of type 2 diabetes: new and future developments in treatment, Lancet 378 (9786) (2011) 182–197.
[7] G. Tao, G. Zhang, W. Chen, C. Yang, Y. Xue, G. Song, S. Qin, A randomized, placebo-controlled clinical trial of hydrogen/oxygen inhalation for non-alcoholic fatty liver disease, Cell. Mol. Med. 26 (14) (2022) 4113–4123.
[8] B. Liu, X. Jiang, Y. Xie, X. Jia, J. Zhang, Y. Xue, S. Qin, The effect of a low dose hydrogen-oxygen mixture inhalation in midlife/older adults with hypertension: a randomized, placebo-controlled trial, Front. Pharmacol. 13 (2022), 1025487.
[9] J. Chen, X. Kong, Y. Lv, S. Qin, X. Sun, F. Mu, T. Lu, K. Xu, "Real world survey" of hydrogen-controlled cancer: a follow-up report of 82 advanced cancer patients, Med. Gas Res. 9 (3) (2019) 115–121.
[10] W. Chen, H. Zhang, S. Qin, Neuroprotective effects of molecular hydrogen: a critical review, Neurosci. Bull. 37 (2021) 389–404.
[11] S. Kajiyama, G. Hasegawa, M. Asano, H. Hosoda, M. Fukui, N. Nakamura, J. Kitawaki, S. Imai, K. Nakano, M. Ohta, T. Adachi, H. Obayashi, T. Yoshikawa, Supplementation of hydrogen-rich water improves lipid and glucose metabolism in patients with type 2 diabetes or impaired glucose tolerance, Nutr. Res. 28 (3) (2008) 137–143.
[12] N. Kamimura, K. Nishimaki, I. Ohsawa, S. Ohta, Molecular hydrogen improves obesity and diabetes by inducing hepatic FGF21 and stimulating energy metabolism in db/db mice, Obesity 19 (7) (2011) 1396–1403.
[13] Q. Wang, X. Zha, Z. Kang, M. Xu, Q. Huang, D. Zou, Therapeutic effects of hydrogen saturated saline on rat diabetic model and insulin resistant model via reduction of oxidative stress, Chin. Med. J. 125 (9) (2012) 1633–1637.
[14] W. Wang, C. Chen, Y. Ying, S. Lv, Y. Wang, X. Zhang, Z. Cai, W. Gu, Z. Li, G. Jiang, F. Gao, Smart PdH@ MnO_2 yolk–shell nanostructures for spatiotemporally synchronous targeted hydrogen delivery and oxygen-elevated phototherapy of melanoma, ACS Nano 16 (4) (2022), 5597−5614.
[15] K. Ge, Z. Li, A. Wang, Z. Bai, X. Zhang, X. Zheng, Z. Liu, F. Gao, An NIR-driven upconversion/C_3N_4/CoP photocatalyst for efficient hydrogen production by inhibiting electron–hole pair recombination for Alzheimer's disease therapy, ACS Nano 17 (3) (2023) 2222–2234.
[16] M. Zhao, Z. Jin, C. Xia, S. Chen, L. Zeng, S. Qin, Q. He, Inhibition of free heme-catalyzed Fenton-like reaction prevents non-alcoholic fatty liver disease by hepatocyte-targeted hydrogen delivery, Biomaterials 301 (2023), 122230.
[17] Y. Zhu, Q. Jiang, L. Zeng, Z. Jin, Q. Xu, J. Chen, Y. Zeng, S. Chen, Q. He, Two-dimensional Mg_2Si nanosheet-enabled sustained hydrogen generation for improved deeply-burned skin repair and regeneration, Adv. Healthcare Mater. 12 (2023), 2201705.
[18] M. Fan, Y. Wen, D. Ye, Z. Jin, P. Zhao, X. Lu, D. Chen, Q. He, Acid-responsive H_2-releasing 2D MgB_2 nanosheet for therapeutic synergy and side effect attenuation of gastric cancer chemotherapy, Adv. Healthcare Mater. 8 (2019), 1900157.
[19] P. Zhao, Z. Jin, Q. Chen, T. Yang, D. Chen, J. Meng, X. Lu, Z. Gu, Q. He, Local generation of hydrogen for enhanced photothermal therapy, Nat. Commun. 9 (2018) 4241.
[20] Z. Jin, Y. Sun, T. Yang, L. Tan, P. Lv, Q. Xu, G. Tao, S. Qin, X. Lu, Q. He, Nanocapsule-mediated sustained H_2 release in the gut ameliorates metabolic dysfunction-associated fatty liver disease, Biomaterials 276 (2021), 121030.
[21] R.K. Goyal, Y. Guo, H. Mashimo, Advances in the physiology of gastric emptying, Neurogast. Motil. 31 (4) (2019), e13546.
[22] R. Schwarz, A. Kaspar, J. Seelig, B. Künnecke, Gastrointestinal transit times in mice and humans measured with ^{27}Al and ^{19}F nuclear magnetic resonance, Magn. Reson. Med. 48 (2) (2002) 255–261.
[23] Z. Kou, P. Zhao, Z. Wang, Z. Jin, L. Chen, B. Su, Q. He, Acid-responsive H_2-releasing Fe nanoparticles for safe and effective cancer therapy, J. Mater. Chem. B 7 (17) (2019) 2759–2765.
[24] B. Liu, J. Xue, Q. Gu, M. Zhao, M. Zhang, M. Wang, Y. Wang, S. Qin, In vivo microelectrode monitoring of real-time hydrogen concentration in different tissues of rats after inhaling hydrogen gas, Med. Gas Res. 12 (3) (2022) 107–112.
[25] W. Zhu, Q. Gu, B. Liu, Y. Si, H. Sun, J. Zhong, Y. Lu, D. Wang, J. Xue, S. Qin, Accurate in vivo real-time determination of the hydrogen concentration in different tissues of mice after hydrogen inhalation, Heliyon 8 (2022), e10778.
[26] B. Liu, Y. Xie, J. Chen, J. Xue, X. Zhang, M. Zhao, X. Jia, Y. Wang, S. Qin, Protective effect of molecular hydrogen following different routes of administration on D-Galactose-induced aging mice, J. Inflamm. Res. 14 (2021) 5541–5550.
[27] J. Xue, M. Zhao, Y. Liu, X. Jia, X. Zhang, Q. Gu, Y. Xie, S. Qin, B. Liu, Hydrogen inhalation ameliorates hepatic inflammation and modulates gut microbiota in rats with high-fat diet-induced non-alcoholic fatty liver disease, Eur. J. Pharmacol. 947 (2023), 175698.
[28] X. Yao, D. Chen, B. Zhao, B. Yang, Z. Jin, M. Fan, G. Tao, S. Qin, W. Yang, Q. He, Acid-Degradable Hydrogen-generating metal-organic framework for overcoming cancer resistance/metastasis and off-target side effects, Adv. Sci. 9 (10) (2022), 2101965.
[29] Q. Xu, S. Chen, L. Jiang, C. Xia, L. Zeng, X. Cai, Z. Jin, S. Qin, W. Ding, Q. He, Sonocatalytic hydrogen/hole-combined therapy for anti-biofilm and infected diabetic wound healing, Natl. Sci. Rev. 10 (2023) nwad063.
[30] B. Wang, P.C. Chandrasekera, J.J. Pippin, Leptin-and leptin receptor-deficient rodent models: relevance for human type 2 diabetes, Curr. Diabetes Rev. 10 (2) (2014) 131–145.